CAI Minghui, XU Liangliang, YANG Tao, HAN Jianwei. A novel magnetic configuration for space radiation active shielding. *Chin. J. Space Sci.*, 2021, **41**(6): 920-927. DOI:10.11728/cjss2021.06.920

A Novel Magnetic Configuration for Space Radiation Active Shielding*

CAI Minghui[1,2] XU Liangliang[1] YANG Tao[1] HAN Jianwei[1,2]

1(*National Space Science Center, Chinese Academy of Sciences, Beijing* 100190)

2(*School of Astronomy and Space Science, University of Chinese Academy of Sciences, Beijing* 100049)

Abstract Space radiation has been identified as the main health hazard to crews involved in manned Mars missions. Active shielding is more effective than passive shielding to the very energetic particles from cosmic rays. Particle motion in a magnetic field is studied based on the single-particle theory and Monte Carlo method. By comparing the shielding efficiency of different magnetic field configurations, a novel active magnetic shielding configuration with lower mass cost and power consumption is proposed for manned Mars missions. The new magnetic configuration can shield 92.8% of protons and 84.4% of alpha particles with $E < 4\,\mathrm{GeV{\cdot}n^{-1}}$, when considering the passive shielding contribution of $10.0\,\mathrm{g{\cdot}cm^{-2}}$ Al Shielding, the required magnetic stiffness can be reduced from 27 Tm to 16 Tm. The detailed analysis of mass cost and power consumption shows that active shielding will be a promising means to protect crews from space radiation exposure in manned Mars missions.

Key words Space radiation, Magnetic shielding, Super conducting magnets, Mars mission

Classified index TM 153, V 4

0 Introduction

Space radiation has been identified as the main health hazard to crews involved in long-term interplanetary missions. In free space to and from Mars, without the protection of the terrestrial magnetic field, the Solar Cosmic Rays (SCR) emitted by Sun and the much more energetic Galactic Cosmic Rays (GCR) originated and accelerated in the galaxy are the two categories to be considered. SCRs usually emitted in Solar Particle Events (SPE) are sporadic and impossible to be forecast. Sometimes SCRs last for several hours up to a few days with a very high flux of energetic protons, which can lead to acute effects, including lethal radiation syndromes. The energy of the GCR is much higher, at least of an order of magnitude, the intensity of their flux is very lower and roughly continuous in time. What is dangerous for human health is the accumulation of their effects on an interval of time of several months or a few years[1]. According to the measurements of the Radiation Assessment Detector (RAD) instrument on the Mars Science Laboratory (MSL) during the cruise to Mars, the average daily radiation dose is about 1.84 mSv; GCRs contributed 95% to the total dose during the journey[2]. Therefore, during the foreseen 500-day mission to and from Mars, the dose due to GCRs will far exceed the limits recommended by the International Commission on Radiological Protection[3]. Passive Shielding in space is problematic because of the huge mass of the needed absorbers, especially when the energetic GCRs are considered[4−6]. As an example, a 400-day transit to and from Mars, without including the surface stay, a minimum of 24 heavy-lift launches of polyethylene at 40.54 tonnes each are needed for the 1977 GCR environment[7].

* Supported by the Strategic Priority Research Program of Chinese Academy of Sciences (XDA17010301)
Received December 22, 2020, Revised October 25, 2021
Corresponding author E-mail: caiminghui@nssc.ac.cn

Active shielding is one promising solution because GCR consists mainly of charged particles. In the active shielding from charged particles are deflected outside the protected volume by using electromagnetic fields in a given configuration. Active shielding concepts have been investigated since the early 1960s, which include the use of electrostatic fields, plasmas, confined magnetic fields, unconfined magnetic fields and mini-magnetospheres. A comprehensive listing of nearly all publications related to the active shield of spacecraft can be found in the article[8] and in the short review given by Townsend[9,10]. Although many technical advances need to be made to make active shielding a reality, they hold the promise of potentially being able to reduce the radiation exposure received by astronauts to acceptable levels, at a significantly lower mass penalty than passive shielding[11,12].

The purpose of this study is to propose a novel active magnetic configuration used to protect crews from space radiation exposure in manned Mars missions. To propose an optimal shielding scheme, the shielding efficiency of different magnetic configurations is compared. What's more, the mass cost, power consumption and assembly mode of the active magnetic configuration are discussed for engineering feasibility analysis.

1 Calculation Method and Results

1.1 GCR flux

The CREME96 model is used in the current analysis to compute the GCR flux in deep-space. The CREME96 model provides the GCR energy spectrum from $1\,\mathrm{MeV{\cdot}n^{-1}}$ to $106\,\mathrm{MeV{\cdot}n^{-1}}$ (n represents nuclear) for elements with $Z = 1$ through $Z = 94$. This study only takes into account elements with $Z = 1$ through $Z = 28$, since the resulting dose equivalent for elements with Z greater than 28 provides a negligible contribution to the total dose equivalent[13]. The GCR spectra used in this analysis is corresponding to the 1977 solar minimum, flux distributions in energy for hydrogen, helium, oxygen, and iron are shown in Figure 1.

1.2 Particle Motion in a Magnetic Field

The motion of charged particles as they pass through a magnetic field is governed by the Lorentz force equation, given by

$$\boldsymbol{F} = q\boldsymbol{v} \times \boldsymbol{B}, \tag{1}$$

where q is the particle's charge, $\boldsymbol{v}$ is the particle's velocity, and $\boldsymbol{B}$ is the magnetic field strength. This force affects particle motion perpendicular to the magnetic field lines, while the velocity component parallel to the magnetic field remains unaffected. Since the energy of GCR particles can reach to $\mathrm{GeV{\cdot}n^{-1}}$, relativistic equations must be utilized. The Lorentz force results in the particle's motion in the plane perpendicular to the magnetic field being circular. The equation for the radius of curvature of a charged particle in a magnetic field, which is also known as the Larmor radius or gyroradius, is given by

$$\boldsymbol{r}_{\mathrm{L}} = \frac{\gamma m_0 v_{\perp}}{qB}, \tag{2}$$

where γ is the Lorentz factor, m_0 is the particle rest mass and $v_{\perp}$ is the particle's velocity component perpendicular to the magnetic field. Eq. (2) demonstrates that as the velocity of a given particle increases, its Larmor radius will also increase, making the particle more difficult to deflect. Additionally, a higher magnetic field strength results in a smaller Larmor radius, causing greater deflection of a given particle.

1.3 Open-ended Cylinder Model

To simplify the complex calculations for determining the GCR flux inside a magnetic field, a finitely long,

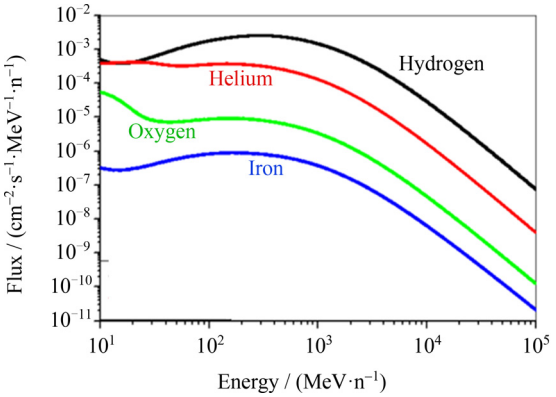

Fig. 1 GCR spectra of four galactic cosmic radiation particles

and cylindrically shaped, solenoid magnetic field model is used[14], as shown in Figure 2. In the "open-ended cylin-der" design, the regions on the ends will be referred to as the "end-cap" regions, there is no magnetic field is present. The area between the two end-cap regions will be referred to as the "barrel" region, there is a uniform magnetic field is present. In our calculations, it is assumed that the length of the active shield is 10 m. Additionally, it is also assumed that the inner radius of the magnetic field is 4 m.

Our calculation is based on the single-particle theory and Monte Carlo method: for each energy, a particle source with iso-tropic velocity is distributed just outside the outer surface of the shield. The particles start randomly just outside the surface of the shield. The total number of particles which traverse the magnetic field and enter the habitat is recorded, using 10 000 trials for each energy. The simulation is carried out with and without a magnetic field for each energy, the shielding efficiency η can be written as

$$\eta = 1 - \frac{n_{\text{in2}}}{n_{\text{in1}}}, \tag{3}$$

where n_{in1} is the particle number entering without field, n_{in2} is the particle number entering with the field. To improve the computational efficiency, the passive shielding contribution of the structural mass to GCR is not considered in this paper.

In the following Figure 3, we present the shielding efficiency calculated results for Protons and alpha-particles. It can be seen from the figure that when the magnetic field thickness L is determined, the shielding efficiency η decreases firstly with the magnetic field intensity B and then increases when the magnetic field intensity B is greater than 4 T, the shielding efficiency increases with the shielding magnetic field thickness L. When the magnetic field intensity B reaches 20 T, the shielding efficiency for Protons and alpha particles is less than 70% and 60%, respectively. Since there is no magnetic field protection at the ends of the solenoid, any charged particle can enter the shield area, resulting in low shielding efficiency.

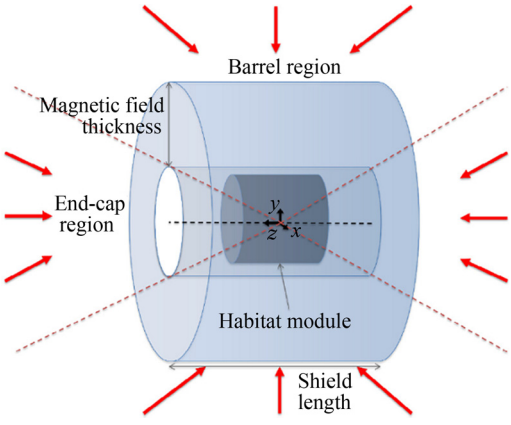

Fig. 2 Open-ended cylinder model

1.4 Close-ended Cylinder Model

To improve the shielding efficiency at the ends, a variety of close-ended cylinder magnetic field configurations are designed. Hoffman magnetic field configuration[15] is shown in Figure 4(a), the barrel region and the end-cap regions are toroidal magnetic fields. A new magnetic field configuration 1A is proposed by increasing the area of the end-cap area and changing the magnetic field direction of the end-cap area, as shown in Figure 4(b).

Four magnetic field structures are proposed in this paper, that is, solenoidal configuration and toroidal configuration magnetic fields are combined in the barrel region and the end-cap regions respectively.

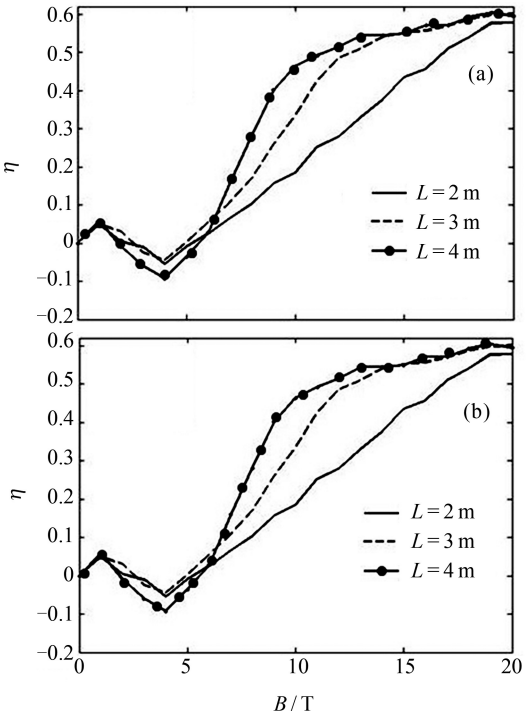

Fig. 3 Shielding efficiency with magnetic field strength and thickness. (a) Proton, (b) alpha particles

Table 1 Magnetic field configurations

Configuration	Barrel region			End-cap regions		
	Shape	Axial length	Thickness	Shape	Radius	Thickness
Hoffman	Toroidal	$Z+2L$	L	Toroidal	r_i	L
1-A	Toroidal	Z	L	Toroidal	r_i+L	L
1-B	Toroidal	$Z+2L$	L	Toroidal	r_i	L
2-A	Solenoidal	Z	L	Toroidal	r_i+L	L
2-B	Solenoidal	$Z+2L$	L	Toroidal	r_i	L
3-A	Solenoidal	Z	L	Solenoidal	r_i+L	L
3-B	Solenoidal	$Z+2L$	L	Solenoidal	r_i	L
4-A	Toroidal	Z	L	Solenoidal	r_i+L	L
4-B	Toroidal	$Z+2L$	L	Solenoidal	r_i	L

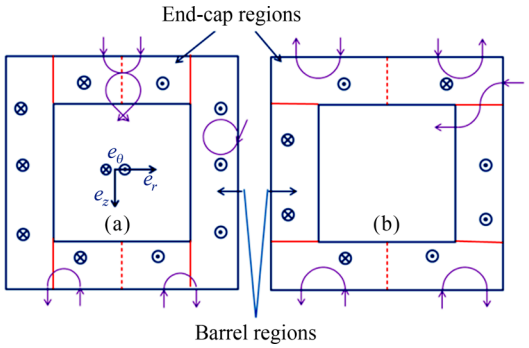

Fig. 4 Magnetic field configurations. (a) Hoffman configuration, (b) configuration 1-A

Further consider whether the end-cap region covers the barrel region, which is divided into group A and group B. Table 1 lists 8 new magnetic field configurations based on Hoffman magnetic field configuration.

In our calculations, it is assumed that the size of the protective zone is $\phi 7\,\mathrm{m}\times 7\,\mathrm{m}$, the magnetic field thickness L is 1.5 m. Then the basic parameters of the shielding magnetic field are as follows, the inner radius of the magnetic field is 3.5 m, the outer radius of the magnetic field is 5 m, the shield length of the magnetic field is 10 m.

The following Figure 5 shows the shielding efficiency for a proton with different magnetic field conditions, including configuration, magnetic field strength, and thickness. It can be seen from the figure, when the magnetic stiffness BL is certain, the shielding effect of increasing the magnetic field intensity B is better than that of increasing the magnetic field thickness L. Compared with the 9 magnetic field configurations listed in Table 3, the group A configuration is better than the group B configurations, and

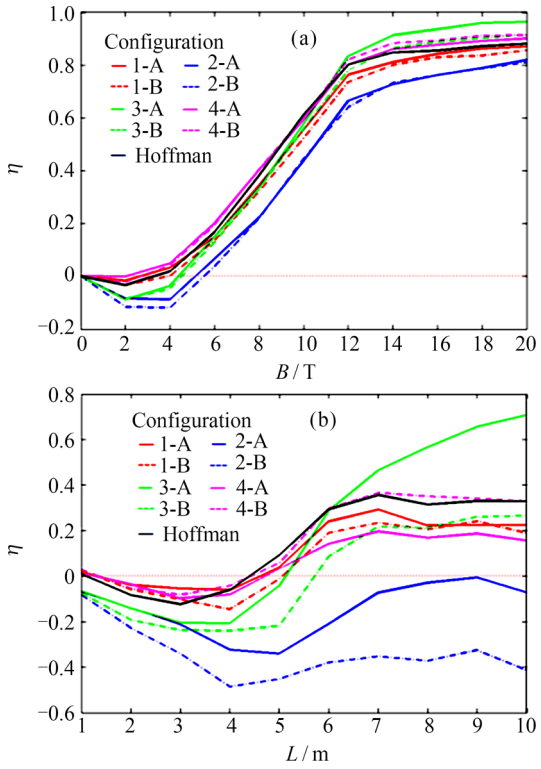

Fig. 5 Shielding efficiency of 9 configurations for a proton with different conditions. (a) Different magnetic field strength, (b) different magnetic field thickness

the shielding effect of the magnetic field configuration 3-A is the best.

Figure 6 shows the proton and alpha particle's energy spectrum after shielding with different magnetic field rigidities in the center of the magnetic field configuration 3-A, respectively. It can be seen from the figures that 96% of protons and 85% of alpha particles with $E<4\,\mathrm{GeV\cdot n^{-1}}$ can be shielded at magnetic field rigidities 27 Tm.

1.5 Calculation of the Realistic Magnetic Field Configurations

The magnetic field configurations discussed above are ideal for assuming uniform magnetic field distribution, but the actual magnetic field distribution is often uneven. The shielding efficiency of the more realistic magnetic shielding configuration is analyzed below, as shown in Figure 7.

Figure 8 shows the shielding effect of the magnetic field configuration shown in Figure 7(a) on proton and alpha particles. It can be seen from the figures that 36.6% of protons and 26.7% of alpha particles with $E < 4\,\mathrm{GeV{\cdot}n^{-1}}$ can be shielded at magnetic field rigidities 27 Tm.

Figure 9 shows the shielding effect of the magnetic field configuration shown in Figure 7(b) on proton and alpha particles. It can be seen from the figures that 80.8% of protons and 65.2% of alpha particles with $E < 4\,\mathrm{GeV{\cdot}n^{-1}}$ can be shielded at magnetic field rigidities 27 Tm.

Considering the practical application of engineering, the entrance, and exit of astronauts must be set aside at both ends of the magnetic field protection zone. Therefore, a more elongated cylinder model is proposed to reduce the effect of the two ends of the magnetic field, as shown in Figure 10. The basic parameters of the shielding magnetic field are as follows, the inner radius of the magnetic field is 2.7 m, the outer radius of the magnetic field is 2.45 m, and the shield length of the magnetic field is 7.7 m.

Figure 11 shows the shielding effect of the magnetic field configuration shown in Figure 10 on proton and alpha particles. It can be seen from the figures that 92.8% of protons and 84.4% of alpha particles with $E < 4\,\mathrm{GeV{\cdot}n^{-1}}$ can be shielded at magnetic field rigidities 27 Tm. Considering the passive shielding

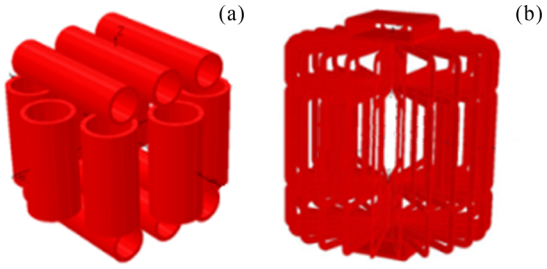

Fig. 7 Realistic magnetic field configurations. (a) Solenoidal configuration, (b) toroidal configuration

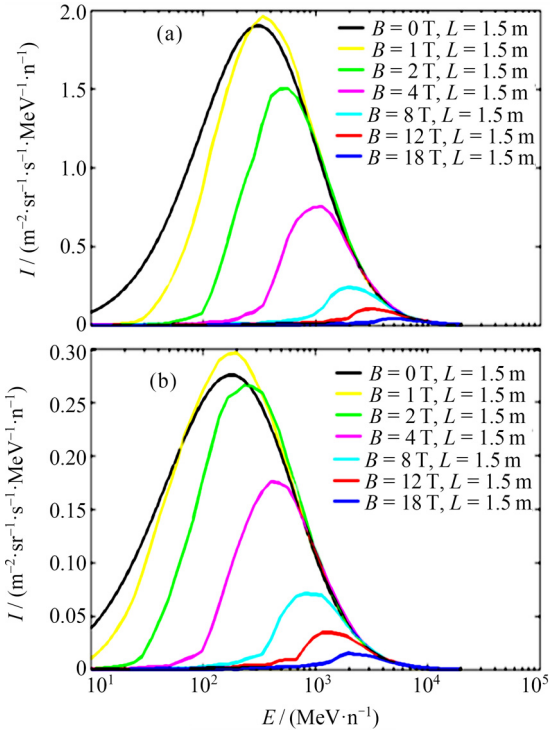

Fig. 6 GCR spectra after shielding with different magnetic field rigidities. (a) Proton, (b) alpha particles

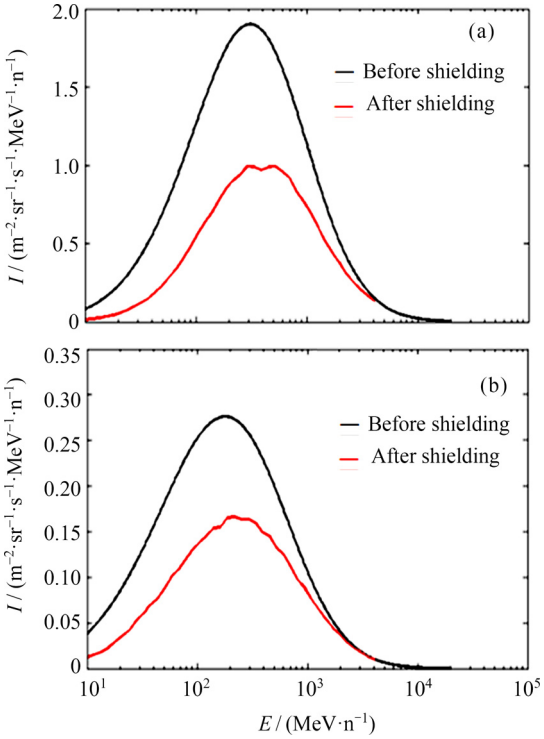

Fig. 8 Shielding effect of the solenoidal configuration. (a) Proton, (b) alpha particles

contribution of 10.0 g·cm^{-2} Al Shielding, the magnetic stiffness can be reduced from 27 Tm to 16 Tm[16].

2 Discussion of Engineering Feasibility

2.1 Mass Analysis

The magnetic field configuration of the presented design consists of three coils; the main parameters of each coil are estimated with the Yttrium-Barium-Copper-Oxide (YBCO) tape conductor, as shown in Table 2.

Detailed mass estimates for each part of the entire superconducting magnetic field system are shown in Table 3, including coils, mechanical structures, and refrigerators. The conductor mass of the magnet is 23.17 tons, the mass of the low- temperature system is 17.27 tons, and the total system mass is 40.44 tons.

2.2 Power Analysis

Magnet system power consumption mainly comes from two aspects, one in the refrigerator, and the other is the magnetic flux pump. A total of 49 Stirling refrigerators are required for the system, of which 48 are used for magnet refrigeration and 1 for high-temperature coil hysteresis loss during excitation. A total of 11.76 kW is required if the rated power of each Stirling refrigerator is 240 W. When the magnet is excited, the input power required for stable operation is greatly reduced, and about 5 kW is needed to cope with local joint heating and loss. The magnetic flux pump is no longer required to be energized after excitation, starting only after the magnetic field decays. At present, the maximum input power of the magnetic flux pump is about 500 W. Therefore, the whole magnet system needs a rated peak power total of about 12.26 kW, and the stable operation of the magnet requires a sustained input power of about 5 kW.

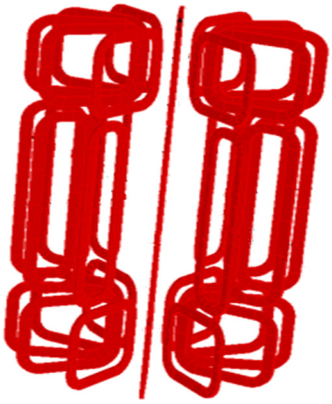

Fig. 10 Optimized magnetic field configuration

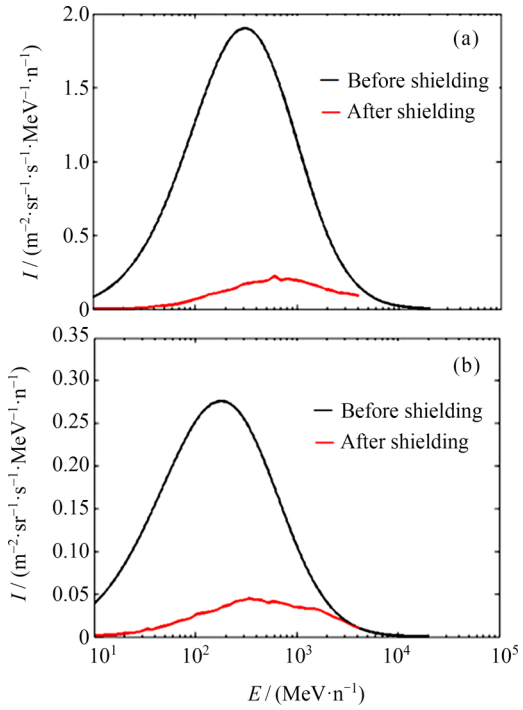

Fig. 9 Shielding effect of the toroidal configuration. (a) Proton, (b) alpha particles

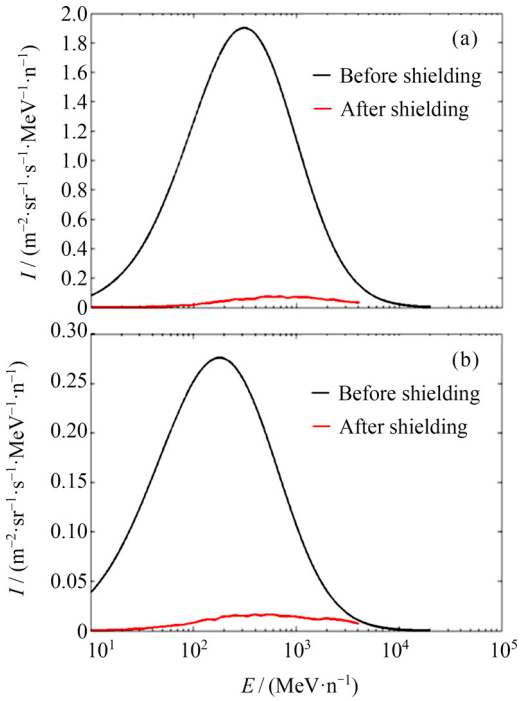

Fig. 11 Shielding effect of the optimized magnetic field configuration. (a) Proton, (b) alpha particles

Table 2 Main Parameters of the superconducting coils with YBCO for Radiation Shield

Parameters	End coil	Central coil	Bottom coil
Temperature/K	4.2	4.2	4.2
Outer height/m	1.7	3.9	1.7
Outer width/m	1.9	1.1	1.9
Inner height/m	1.3	3.5	1.3
Inner width/m	1.5	0.7	1.5
Unilateral width/m	0.2	0.2	0.2
Unilateral thickness/m	0.06	0.06	0.06
Inner fillet radius/m	0.25	0.25	0.25
Outer fillet radius/m	0.25	0.25	0.25
Operational current/($A\cdot m^{-2}$)	6×10^8	4.8×10^8	6×10^8
Inductance/H	2820	3980	2820
Stored energy/MJ	81.22	73.36	81.22
Number of coils	12	12	12
Average magnetic field/T	13	10	13
Peak magnetic field/T	18	15	18
Conductor dosage/m^3	0.83	1.23	0.83
Single coil mass/kg	554	823	554
Mass/kg	6648	9876	6648

Table 3 Detailed mass estimates for each part of the entire superconducting magnetic field system

Constituent part	Material	Number	Mass/kg
Circumferential support rod	titanium	48	163.01
Transverse support rod	aluminum	144	403.20
Longitudinal support rod	aluminum	168	213.36
Large support seat	aluminum	288	86.40
Small support seat	aluminum	624	117.94
Refrigerator	composite	48	148.80
Refrigeration connector	aluminum	48	15.46
Longitudinal coil seal	aluminum	12	752.64
Longitudinal coil seal plate	aluminum	24	5734.80
Inner support ring1	aluminum	2	189.46
Longitudinal coil heat pipe	aluminum	12	54.12
Horizontal coil seal	aluminum	24	1057.2
Line seal plate	aluminum	48	5251.2
Inner support ring2	titanium	4	95.12
Horizontal coil heat pipe	aluminum	12	69.48
Connect the heat pipeline	aluminum	36	4.32
End coil	YBCO	12	6648
End skeleton	brass	12	851.64
Central coil	YBCO	12	9876
Central skeleton	brass	12	1212.6
Bottom coil	YBCO	12	6648
Bottom skeleton	brass	12	851.64
Total mass			40 444

2.3 Mission Analysis

Besides the mass and power required for the superconducting magnetic systems, it must be considered the complexity of the mission. Two scenarios can

be chosen: (i) the active system is launched together with habitat by one launch; and (ii) the active system is launched separately from the habitat by one or more launches, and hereafter assembled in space around the habitat. Based on current rocket launch capabilities and mass costs of the superconducting magnetic systems, the most likely launch option is to assemble in orbit after multiple launches.

3 Conclusions

With the development of high temperature superconducting technology, active shielding will be a promising means to protect crews from space radiation exposure in manned Mars missions. A novel active magnetic configuration with lower mass cost and power consumption is proposed in the paper, the main conclusions are as follows:

(1) The new active magnetic configuration can shield 92.8% of protons and 84.4% of alpha particles with $E < 4\,\mathrm{GeV{\cdot}n^{-1}}$ at magnetic field rigidities 27 Tm. What's more, considering the passive shielding contribution of $10.0\,\mathrm{g{\cdot}cm^{-2}}$ Al Shielding, the magnetic stiffness can be reduced from 27 Tm to 16 Tm.

(2) The active magnetic system has a total mass of 40.44 tons, including coils, mechanical structures, and refrigerators. The active magnet system needs a rated peak power total of about 12.26 kW, and the stable operation of the magnet requires a sustained input power of about 5 kW.

(3) The detailed analysis of mass cost and power consumption shows that active shielding will be a promising means to protect crews from space radiation exposure in manned Mars missions.

References

[1] SPILLANTINI P. Superconducting magnets and mission strategies for protection from ionizing radiation in interplanetary manned missions and interplanetary habitats [J]. *Acta Astronaut.*, 2011, **68**(9/10): 1430-1439

[2] ZEITLIN C, HASSLER D M, CUCINOTTA F A, *et al.* Measurements of energetic particle radiation in transit to Mars on the Mars Science Laboratory [J]. *Science*, 2013, **340**(6136): 1080-1084

[3] CHARLES M W. ICRP Publication 103: recommendations of the ICRP [J]. *Radiat. Protect. Dosim.*, 2008, **4**: 1618

[4] BARTHEL J, SARIGUL-KLIJN N. A review of radiation shielding needs and concepts for space voyages beyond Earth's magnetic influence [J]. *Prog. Aeros. Sci.*, 2019, **110**: 100553.1-100553.16

[5] MANNING B, SINGLETERRY R. Radiation engineering analysis of shielding materials to assess their ability to protect astronauts in deep space from energetic particle radiation [J]. *Acta Astron.*, 2020, **171**. DOI: 10.1016/j.actaastro.2020.02.020

[6] NAITO M, KODAIRA S, OGAWARA R, *et al.* Investigation of shielding material properties for effective space radiation protection [J]. *Life Sci. Space Res.*, 2020, **26**. DOI: 10.1016/j.lssr.2020.05.001

[7] SINGLETERRY R C. Radiation engineering analysis of shielding materials to assess their ability to protect astronauts in deep space from energetic particle radiation [J]. *Acta Astron.*, 2013, **91**: 49-54

[8] SUSSINGHAM J C, WATKINS S A, COCKS F H. Forty years of development of active systems for radiation protection of spacecraft [J]. *J. Astron. Sci.*, 1999, **47**(3): 165-175

[9] TOWNSEND L W. Overview of active methods for shielding spacecraft from energetic space radiation [J]. *Phys. Medica*, 2001, **17**(1): 84

[10] SPILLANTINI P. Manned exploration and exploitation of solar system: passive and active shielding for protecting astronauts from ionizing radiation-a short overview [J]. *Acta Astronaut.*, 2014, **104**(2): 509-515

[11] WASHBURN S A, BLATTNIG S R, SINGLETERRY R C, *et al.* Active magnetic radiation shielding system analysis and key technologies [J]. *Life Sci. Space Res.*, 2015, **4**: 22-34

[12] VUOLO M, GIRAUDO M, MUSENICH R, *et al.* Monte Carlo simulations for the space radiation superconducting shield project (SR2S) [J]. *Life Sci. Space Res.*, 2016, **8**: 22-29

[13] SIMPSON J A. Elemental and isotopic composition of the galactic cosmic rays [J]. *Ann. Rev. Nucl. Part*, 2003, **33**(1): 323-382

[14] WASHBURN S A, BLATTNIG S R, SINGLETERRY R C, *et al.* Analytical-HZETRN model for rapid assessment of active magnetic radiation shielding [J]. *Adv. Space Res.*, 2014, **53**(1): 8-17

[15] HOFFMAN J, FISHER P, BATISHCHEV O. Use of superconducting magnet technology for astronauts radiation protection [C]//NIAC Phase I Fellows Meeting Atlanta. Georgia: 2005

[16] MUSENICH R, CALVELLI V, FARINON S, *et al.* Space radiation superconducting shields [J]. *J. Phys. Conf.*, 2014, **507**(3): 032033